Pyruvate kinase from plasmodium falciparum

Pyruvate kinase from *Plasmodium falciparum*: structural and kinetic insights into the allosteric mechanism

Wenhe Zhong[1,2], Kuohan Li[3,4], Qixu Cai[5], Jingjing Guo[6], Meng Yuan[7], Yee Hwa Wong[2,4], Malcolm D. Walkinshaw[8], Linda A. Fothergill-Gilmore[8], Paul A.M. Michels[8], Peter C. Dedon[1,9,*] and Julien Lescar[1,2,4,*]

[1]Antimicrobial Resistance Interdisciplinary Research Group, Singapore-MIT Alliance for Research and Technology, 1 CREATE Way, 138602, Singapore.

[2]NTU Institute of Structural Biology, Nanyang Technological University, 636921, Singapore.

[3]Lee Kong Chian School of Medicine, Nanyang Technological University, 59 Nanyang Drive, 636921, Singapore.

[4]School of Biological Sciences, Nanyang Technological University, 60 Nanyang Drive, 637551, Singapore.

[5]Division of Life Science, State Key Laboratory of Molecular Neuroscience, Hong Kong University of Science and Technology, Clear Water Bay, Kowloon, Hong Kong, China.

[6]College of Life Sciences, Nanjing Agricultural University, Nanjing, 210095, China.

[7]Department of Integrative Structural and Computational Biology, The Scripps Research Institute, La Jolla, CA 92037, USA

[8]Institute of Quantitative Biology, Biochemistry and Biotechnology, University of Edinburgh, King's Buildings, Edinburgh EH9 3BF, UK.

[9]Department of Biological Engineering and Center for Environmental Health Sciences, Massachusetts Institute of Technology, Cambridge, MA 02139, USA.

*Corresponding Authors

Email: pcdedon@mit.edu (P.C.D.) and julien@ntu.edu.sg (J.L.).

Key words:

Allostery, kinetics, kinases, crystal structures

Abbreviations:

PYK, pyruvate kinase

Pf, *Plasmodium falciparum*

Lm, *Leishmania mexicana*

F16BP, fructose 1,6-bisphosphate

F26BP, fructose 2,6-bisphosphate

G6P, glucose 6-phosphate

OX, oxalate

Abstract

During its intra-erythrocytic growth phase, the malaria parasite *Plasmodium falciparum* relies heavily on glycolysis for its energy requirements. Pyruvate kinase (PYK) is essential for regulating glycolytic flux and for ATP production, yet the allosteric mechanism of *P. falciparum* PYK (*Pf*PYK) remains poorly understood. Here we report the first crystal structure of *Pf*PYK in complex with substrate analogues oxalate and the ATP product. Comparisons of *Pf*PYK structures in the active R-state and inactive T-state reveal a 'rock-and-lock' allosteric mechanism regulated by rigid-body rotations of each subunit in the tetramer. Kinetic data and structural analysis indicate glucose 6-phosphate is an activator by increasing the apparent maximal velocity of the enzyme. Intriguingly, the trypanosome drug suramin inhibits *Pf*PYK, which points to glycolysis as a set of potential therapeutic targets against malaria.

Introduction

Plasmodium falciparum is the etiologic agent of the most severe forms of malaria, which caused ~435,000 deaths in 2017 [1]. During the intra-erythrocytic stage of its life cycle, the malaria parasite depends heavily on glycolysis for ATP production[2,3], which makes glycolytic enzymes natural anti-malaria drug targets [4,5]. The activity of pyruvate kinase (PYK, **EC 2.7.1.40**) catalyzes the last step of glycolysis to produce ATP and is regulated by several physiological effectors. Three allosteric sites have been identified in PYKs: the canonical site, which is generally regulated by fructose 1,6-bisphosphate (F16BP)[6-8], fructose 2,6-bisphosphate (F26BP) [9,10], or AMP [11]; the sugar-monophosphate site found in mycobacteria [11]; and the amino-acid site found in cancer cells[12,13].

Two PYK isoenzymes have been discovered in *P. falciparum* [4,14]: PYK-I (canonical PYK, (UniProtKB C6KTA4) mainly involved in glycolysis and PYK-II that localizes to the apicoplast and correlates with lipid synthesis. Here, unless stated otherwise, *Pf*PYK stands for *P. falciparum* PYK-I. About 15 years ago, Chan *et al.* were first to clone the gene for *Pf*PYK and expressed it as a recombinant *Pf*PYK enzyme[15]. However, the kinetic characterization was performed on GST-tagged *Pf*PYK. Given its large size (~26 kDa), it is likely that the GST tag partially hindered or affected conformational changes occurring in the *Pf*PYK tetramer (~55 kDa per monomer), which are crucial for allosteric regulation. So, a structure/function study of the native enzyme remains to be done. Here, we report biochemical and structural studies of an untagged *Pf*PYK that reveal a "rock-and-lock" allosteric mechanism regulated by rigid-body rotations and a B-domain motion controlled by active-site ligand binding.

Results and discussion

Untagged *Pf*PYK protein production

*Pf*PYK was purified from an *Escherichia coli* expression system and the N-terminal His_6-tag was cleaved to generate a fully untagged *Pf*PYK (See Materials and methods). The untagged *Pf*PYK shows similar activity to the GST-tagged *Pf*PYK with a k_{cat} value of 248 ± 2.1 s^{-1} *versus* 257 s^{-1}, respectively

[15] (**Table 1**). For the substrate phosphoenolpyruvate (PEP), the untagged *Pf*PYK displayed sigmoidal kinetics in the absence of effector, with a $S_{0.5}$ value of 0.33 ± 0.01 mM and a Hill coefficient (h) of 1.4 ± 0.1, indicating positive cooperativity. Likewise, the untagged enzyme showed sigmoidal kinetics with respect to its substrate ADP with a $S_{0.5}$ value of 0.24 ± 0.01 mM and a h of 1.6 ± 0.1. In contrast, the GST-tagged *Pf*PYK exhibits hyperbolic kinetics with respect to both substrates under similar assay conditions [15]. This difference may be due to the presence of a GST tag in this previous study.

The activation of untagged *Pf*PYK

We then investigated the enzymatic effects of a series of metabolites on *Pf*PYK (**Fig. 1A**). In agreement with previous findings by Chan *et al.*[15], we did not observe effects from "canonical" activators such as F16BP and F26BP. Interestingly, glucose 6-phosphate (G6P) showed a notable PYK activation, while the known inhibitor oxalate (OX) significantly inhibited the enzyme activity (IC_{50} ~149 μM). The binding of G6P and OX, which potentially lock the enzyme in its active state, increased the thermal stability of the enzyme (**Fig. 1B**). In the presence of G6P at a concentration of 5 mM, both the enzyme activity (k_{cat}) and the catalytic efficiency ($k_{cat}/S_{0.5}$) of *Pf*PYK were enhanced by ~1.5-fold without affecting the affinity and cooperativity towards the PEP substrate (**Table 1**; **Fig. 1C**). This suggests that *Pf*PYK could be a V-type allosteric enzyme with respect to G6P. One of the phosphate binding motifs at the canonical effector site is highly conserved and is named "PO_4-2 motif" (**Fig. S1**; **Table S1**). Therefore, we performed *in silico* docking of the activator G6P to the canonical effector site and found that the phosphate group of G6P formed a number of favorable interactions with the PO_4-2 motif (**Fig. 1D**). In contrast, citrate slightly decreased the affinity for the PEP substrate, with no obvious change in the apparent k_{cat} (**Table 1**). It is noteworthy that citrate at 2 mM inhibited GST-tagged *Pf*PYK activity by over 90% [16].

Crystal structure of *Pf*PYK

The only crystal structure of *Pf*PYK in the inactive T-state was deposited to the Protein Data Bank by the Structural Genomics Consortium (SGC) (PDB ID: 3KHD). No report describing the structure and allosteric mechanism was published, which might be due to the lack of an active R-state structure for

comparison. Here, we successfully determined the crystal structure of *Pf*PYK in the R-state with oxalate (substrate PEP analogue) and ATP bound at the active site (**Table 2**). Similar to other protozoan PYK structures [9,17], *Pf*PYK adopts a tetrameric architecture formed by identical subunits with four domains (N-terminus, A, B and C domains) (**Fig. 2A**). The active site is located in the cleft between the A-domain and the lid-like B-domain, while the C-domain harbors a canonical effector site. While the activator G6P was present in the crystallization buffer, no electron density for the G6P moiety was observed. Thus, in the absence of the activator, the effector loop (residues 493-502) was flexible and could not be traced with confidence.

Allostery of *Pf*PYK

The allosteric mechanism was analyzed at the level of quaternary protein structure by superposing the R-state tetramer structure (PDB ID: 6KSH) onto the inactive T-state tetramer structure (PDB ID: 3KHD), excluding the mobile B domains. In agreement with the "rocking motion" mechanism identified in human M2PYK[12], as well as PYKs from trypanosomes [9,10,18] and mycobacteria [11], the superposition suggests that each subunit of the tetramer simultaneously undergoes a 9° rigid-body (AC-core) rotation concomitant with the T- to-R-state transition (**Fig. 2B**). We next explored the determinants of these concerted rigid-body rotations during the allosteric interconversion between the T- and R-state (**Fig. 2C, D**). Similar to trypanosomatid PYKs [9,10,18], several additional hydrogen bonds and salt bridges that lock the tetramer in the R-state form across the C-C interface of *Pf*PYK, resulting in a larger interface area (**Tables S2, S3**). Similar interfacial changes were also found at the A-A interface. However, as the effector loop from the *Pf*PYK structure was poorly defined in the electron density map, we were not able to confirm a role for this effector loop in the observed rigid-body rotations, if any. Binding of the active-site ligand oxalate triggers a conformational change ("rock") toward its more thermally-stable R-state ("lock")[9,11]. In *Pf*PYK, when the enzyme was mixed with oxalate alone or in the presence of G6P and ATP, the thermal stability increased slightly ($\Delta T_m = \sim 1$ °C), suggesting that the R-state conformation is more stable. This agrees with the structurally observed additional interface interactions (**Fig. 1B**).

It is now well established that the lid-like B-domain of PYK can adopt multiple conformations regulated by the active-site ligands [9,11]. By superposition of the AC-cores from the R-state (PDB ID: 6KSH) and T-state monomer (PDB ID: 3KHD), we found that the binding of oxalate and ATP caused the B-domain to rotate 40° toward the A-domain compared with the free T-state form (**Fig. 3A**, **B**). The closed conformation of the B-domain in OX/ATP-bound *Pf*PYK was mainly stabilized by the interactions between ATP and the enzyme (**Fig. 3C**). In the open conformation, the B-domain residues Arg109 and Lys191 no longer form interactions with ATP.

Suramin inhibition on *Pf*PYK

Having established *Pf*PYK kinetics and OX/ATP-bound structure, we next assessed the effect of the trypanosome drug suramin [19] on *Pf*PYK in order to explore the possibility of alternative treatments for malaria. Suramin was found to inhibit trypanosomatid PYKs by competing with the ADP substrate [20], which was also observed in *Pf*PYK (**Fig. 4A, B**). The proposed binding mode of suramin shown in **Fig. 4C** could lead to the design of new *Pf*PYK inhibitors.

The design of selective inhibitors against *Pf*PYK was hindered by limited structure illustration and its allosteric regulation study. More than 10 years have elapsed since the first crystal structure of *Pf*PYK at ligand-free inactive state was reported (PDB ID: 3KHD). Unfortunately, the scientific report of *Pf*PYK structure was unavailable in literatures until now. Furthermore, the production of stable and active untagged *Pf*PYK seems to be a challenge where the published kinetics of *Pf*PYK was studied in its GST-tagged form [15]. Here we report modified protocols for the overexpression and purification of untagged *Pf*PYK and its crystallization, which enabled the study of kinetics and determination of its X-ray crystal structure in complex with active-site ligands. Remarkably, we have shown evidence for a unique V-type activation of *Pf*PYK by non-canonical effector G6P. In addition to our findings in trypanosome PYKs [9,10,18], the rigid-body rotation was also found in *Pf*PYK allosteric mechanism. However, it is still unclear whether activator G6P is involved in this conformational change due to the lack of G6P-bound *Pf*PYK structure.

Materials and methods

Details on the enzyme production. kinetics and biophysical analyses can be found in the **Supporting Information**.

Crystallization and data collection

The crystallisation experiments were performed by the vapour-diffusion method using the hanging-drop technique at 4 °C. The drops were equilibrated against a reservoir filled with 1 ml well solution. To co-crystallise *Pf*PYK with the PEP analogue oxalate (OX), product ATP and activator G6P, 1.0 µl protein solution was mixed with 0.5 µl ligand solution (20 mM) and incubated at room temperature for 1-2 minutes. Then 1.5 µl well solution was added to the mixture for crystallisation. Oxalate is a structural analogue of the enolate form of pyruvate and has been generally used in crystallisation conditions to stabilise PYK in the active R-state [10,18]. The well solution consisted of 12% PEG 8000, 10-20% glycerol, 50 mM TEA buffer pH 7.2, 100 mM KCl, 50 mM $MgCl_2$.

X-ray intensity data for the crystal of *Pf*PYK was collected at the Australian Synchrotron (Australia). The dataset was from a single crystal flash-cooled in liquid nitrogen at 100 K. Data were then processed with MOSFLM [21] and scaled with AIMLESS [22,23]. The data-collection and processing statistics are summarised in **Table 2**.

Structure determination

The R-state *Pf*PYK structure was solved by molecular replacement using the program Phaser [24]. The initial search model (*Pf*PYK monomer) for the molecular-replacement experiment was obtained from the deposited T-state *Pf*PYK (PDB ID: 3KHD). The structure was manually adjusted using Coot [25] followed by several cycles of restrained refinement in Autobuster [26]. Where appropriate, water molecules and ligands were added to the structure and TLS refinement was applied at later stage of refinement. Ligands OX and ATP were clearly identified and modeled, however, G6P density was not observed in the structure.

The quality of the structures was assessed using the MOLPROBITY server [27], and the figures were generated using PyMOL [28]. The data processing and refinement statistics are summarised in **Table 2**. The structure factors and coordinates for *Pf*PYK-OX/ATP have been deposited in the RCSB Protein Data Bank as PDB entry 6KSH.

Structure analysis

The program Superpose [29] in the CCP4 [30] suite was used to calculate the allosteric rigid-body rotations and B-domain movements from the superposition of T-state and R-state tetramers as described previously [18]. Both RMS differences and rotation matrices were calculated in the superposition process [18].

Molecular modelling

Molecular modelling was employed to explore the interaction between *Pf*PYK and G6P. The receptor was prepared in Chimera v1.11.2 [31] by removing water molecules, fixing non-standard residues, and adding hydrogen and charges using the ff14SB force field [32]. Then, AutoDock Vina v1.1.2 [33] was employed for docking G6P to the effector site. The ligand was treated as flexible while the protein was treated as rigid. A search space (25×25×25 $Å^3$) was defined with the centre of mass of ligand in the binding site as the centre.

Acknowledgements

We are grateful to Dr. Ghader Bashiri from The University of Auckland (New Zealand) for the gift of the vector pYUB28b. This research was supported by the National Research Foundation of Singapore through the Singapore-MIT-Alliance for Research and Technology (SMART) Antimicrobial Resistance (AMR) research program, and a SMART Postdoctoral Fellowship (W.Z.). During the course of this study, the J.L. lab was supported by grant NMRC/CBRG/0073/2014.

Declaration of competing interest

The authors declare no competing financial interest.

Author Contributions

W.Z. designed the studies and carried out the biochemical and biophysical assays, analyzed diffraction data and refined structures, and drafted the manuscript; K.L. carried out enzyme and biophysical assays, and refined structures; J.G. carried out computational docking; Q.C. and M. Y. analyzed diffraction data; M.D.W., L.A.F.-G., P.A.M., P.C.D., and J.L. analyzed data and coordinated the studies. All authors participated in writing the manuscript.

Supporting information

Additional supporting information may be found online in the Supporting Information section at the end of the article.

References

[1] Geneva: World Health Organization, World Malaria Report 2018, 2018. https://apps.who.int/iris/bitstream/handle/10665/275867/9789241565653-eng.pdf?ua=1.

[2] N. Lang-Unnasch, A.D. Murphy, Metabolic changes of the malaria parasite during the transition from the human to the mosquito host, Annu. Rev. Microbiol. 52 (1998) 561–590. doi:10.1146/annurev.micro.52.1.561.

[3] I.W. Sherman, Biochemistry of Plasmodium (malarial parasites), Microbiol. Rev. 43 (1979) 453–495.

[4] M. Chan, D.S.H. Tan, T.S. Sim, Plasmodium falciparum pyruvate kinase as a novel target for antimalarial drug-screening, Travel Medicine and Infectious Disease. 5 (2007) 125–131. doi:10.1016/j.tmaid.2006.01.015.

[5] G. Penkler, W. Adams, M. Rautenbach, D.C. Palm, J.L. Snoep, Construction and validation of a detailed kinetic model of glycolysis in Plasmodium falciparum, The FEBS Journal. 282 (2015) 1481–1511. doi:10.1111/febs.13237.

[6] E.B. Waygood, B.D. Sanwal, The control of pyruvate kinases of Escherichia coli. I. Physicochemical and regulatory properties of the enzyme activated by fructose 1,6-diphosphate, J. Biol. Chem. 249 (1974) 265–274.

[7] M.S. Jurica, A. Mesecar, P.J. Heath, W. Shi, T. Nowak, B.L. Stoddard, The allosteric regulation of pyruvate kinase by fructose-1,6-bisphosphate, Structure. 6 (1998) 195–210. doi:10.1016/S0969-2126(98)00021-5.

[8] J.D. Dombrauckas, B.D. Santarsiero, A.D. Mesecar, Structural basis for tumor pyruvate kinase M2 allosteric regulation and catalysis, Biochemistry. 44 (2005) 9417–9429. doi:10.1021/bi0474923.

[9] H.P. Morgan, W. Zhong, I.W. McNae, P.A.M. Michels, L.A. Fothergill-Gilmore, M.D. Walkinshaw, Structures of pyruvate kinases display evolutionarily divergent allosteric strategies, Royal Society Open Science. 1 (2014) 140120–140120. doi:10.1098/rsos.140120.

[10] W. Zhong, H.P. Morgan, I.W. McNae, P.A.M. Michels, L.A. Fothergill-Gilmore, M.D. Walkinshaw, `In crystallo' substrate binding triggers major domain movements and reveals

magnesium as a co-activator of Trypanosoma brucei pyruvate kinase, Acta Crystallogr D Biol Crystallogr. 69 (2013) 1768–1779. doi:10.1107/S0907444913013875.

[11] W. Zhong, L. Cui, Q. Cai, P. Ho, M. Yuan, A.E. Sahili, et al., Allosteric pyruvate kinase-based "logic gate" synergistically senses energy and sugar levels in Mycobacterium tuberculosis, Nature Communications. 8 (2017) 693. doi:10.1038/s41467-017-02086-y.

[12] H.P. Morgan, F.J. O'Reilly, M.A. Wear, J.R. O'Neill, L.A. Fothergill-Gilmore, T. Hupp, et al., M2 pyruvate kinase provides a mechanism for nutrient sensing and regulation of cell proliferation, Proc. Natl. Acad. Sci. U.S.a. 110 (2013) 5881–5886. doi:10.1073/pnas.1217157110.

[13] B. Chaneton, P. Hillmann, L. Zheng, A.C.L. Martin, O.D.K. Maddocks, A. Chokkathukalam, et al., Serine is a natural ligand and allosteric activator of pyruvate kinase M2, Nature. 491 (2012) 458–462. doi:10.1038/nature11540.

[14] T. Maeda, T. Saito, O.S. Harb, D.S. Roos, S. Takeo, H. Suzuki, et al., Pyruvate kinase type-II isozyme in Plasmodium falciparum localizes to the apicoplast, Parasitol. Int. 58 (2009) 101–105. doi:10.1016/j.parint.2008.10.005.

[15] M. Chan, T.-S. Sim, Functional analysis, overexpression, and kinetic characterization of pyruvate kinase from Plasmodium falciparum, Biochemical and Biophysical Research Communications. 326 (2004) 188–196. doi:10.1016/j.bbrc.2004.11.018.

[16] R.L. Burton, S. Chen, X.L. Xu, G.A. Grant, Transient kinetic analysis of the interaction of L-serine with Escherichia coli D-3-phosphoglycerate dehydrogenase reveals the mechanism of V-type regulation and the order of effector binding, Biochemistry. 48 (2009) 12242–12251. doi:10.1021/bi901489n.

[17] R. Bakszt, A. Wernimont, A. Allali-Hassani, M.W. Mok, T. Hills, R. Hui, et al., The crystal structure of Toxoplasma gondii pyruvate kinase 1, PLoS ONE. 5 (2010) e12736. doi:10.1371/journal.pone.0012736.

[18] H.P. Morgan, I.W. McNae, M.W. Nowicki, V. Hannaert, P.A.M. Michels, L.A. Fothergill-Gilmore, et al., Allosteric mechanism of pyruvate kinase from Leishmania mexicana uses a

rock and lock model, J. Biol. Chem. 285 (2010) 12892–12898. doi:10.1074/jbc.M109.079905.

[19] F. Hawking, Suramin: with special reference to onchocerciasis, Adv Pharmacol Chemother. 15 (1978) 289–322.

[20] H.P. Morgan, I.W. McNae, M.W. Nowicki, W. Zhong, P.A.M. Michels, D.S. Auld, et al., The trypanocidal drug suramin and other trypan blue mimetics are inhibitors of pyruvate kinases and bind to the adenosine site, J. Biol. Chem. 286 (2011) 31232–31240. doi:10.1074/jbc.M110.212613.

[21] T.G.G. Battye, L. Kontogiannis, O. Johnson, H.R. Powell, A.G.W. Leslie, iMOSFLM: a new graphical interface for diffraction-image processing with MOSFLM, Acta Crystallogr D Biol Crystallogr. 67 (2011) 271–281. doi:10.1107/S0907444910048675.

[22] P. Evans, IUCr, Scaling and assessment of data quality, Acta Crystallogr D Biol Crystallogr. 62 (2006) 72–82. doi:10.1107/S0907444905036693.

[23] P.R. Evans, G.N. Murshudov, IUCr, How good are my data and what is the resolution? Acta Crystallogr D Biol Crystallogr. 69 (2013) 1204–1214. doi:10.1107/S0907444913000061.

[24] A.J. McCoy, R.W. Grosse-Kunstleve, P.D. Adams, M.D. Winn, L.C. Storoni, R.J. Read, Phaser crystallographic software, J Appl Crystallogr. 40 (2007) 658–674. doi:10.1107/S0021889807021206.

[25] P. Emsley, K. Cowtan, Coot: model-building tools for molecular graphics, Acta Crystallogr D Biol Crystallogr. 60 (2004) 2126–2132. doi:10.1107/S0907444904019158.

[26] Exploiting structure similarity in refinement: automated NCS and target-structure restraints in BUSTER, Acta Crystallogr D Biol Crystallogr. 68 (2012) 368–380. doi:10.1107/S0907444911056058.

[27] I.W. Davis, A. Leaver-Fay, V.B. Chen, J.N. Block, G.J. Kapral, X. Wang, et al., MolProbity: all-atom contacts and structure validation for proteins and nucleic acids, Nucl. Acids Res. 35 (2007) W375–W383. doi:10.1093/nar/gkm216.

[28] W.L. DeLano, The PyMOL Molecular Graphics System (2002) DeLano Scientific, San Carlos, CA, USA, Computer Program, 2002.

[29] E. Krissinel, K. Henrick, Secondary-structure matching (SSM), a new tool for fast protein structure alignment in three dimensions, Acta Crystallogr D Biol Crystallogr. 60 (2004) 2256–2268. doi:10.1107/S0907444904026460.

[30] M.D. Winn, C.C. Ballard, K.D. Cowtan, E.J. Dodson, P. Emsley, P.R. Evans, et al., Overview of the CCP4 suite and current developments, Acta Crystallogr D Biol Crystallogr. 67 (2011) 235–242. doi:10.1107/S0907444910045749.

[31] E.F. Pettersen, T.D. Goddard, C.C. Huang, G.S. Couch, D.M. Greenblatt, E.C. Meng, et al., UCSF Chimera--a visualization system for exploratory research and analysis, 25 (2004) 1605–1612. doi:10.1002/jcc.20084.

[32] J.A. Maier, C. Martinez, K. Kasavajhala, L. Wickstrom, K.E. Hauser, C. Simmerling, ff14SB: Improving the Accuracy of Protein Side Chain and Backbone Parameters from ff99SB, 11 (2015) 3696–3713. doi:10.1021/acs.jctc.5b00255.

[33] O. Trott, A.J. Olson, AutoDock Vina: improving the speed and accuracy of docking with a new scoring function, efficient optimization, and multithreading, 31 (2010) 455–461. doi:10.1002/jcc.21334.

Table 1. Kinetic properties of *Pf*PYK and the effects of modulators[a]

Ligand	Kinetic parameter	Modulator		
		None	+G6P[b]	+citrate[b]
PEP	$S_{0.5}$ (mM)	0.33 ± 0.01	0.35 ± 0.02	0.41 ± 0.01
	Hill coefficient, h	1.4 ± 0.1	1.5 ± 0.1	1.4 ± 0.1
	k_{cat} (s^{-1})	248 ± 2	383 ± 7	296 ± 3
	$k_{cat}/S_{0.5}$ ($s^{-1}\cdot mM^{-1}$)	752	1094	722
ADP	$S_{0.5}$ (mM)	0.24 ± 0.01	nd[c]	nd
	Hill coefficient, h	1.6 ± 0.1	nd	nd
	k_{cat} (s^{-1})	246 ± 3	nd	nd
	$k_{cat}/S_{0.5}$ ($s^{-1}\cdot mM^{-1}$)	1025	nd	nd
Suramin	IC_{50} (μM)		128 ± 14	
Oxalate	IC_{50} (μM)		150 ± 11	

[a] Data represent mean ± SD for three replicates
[b] The concentrations of modulators are: G6P - 5 mM, citrate - 5 mM
[c] nd, not determined

Table 2. Data collection and refinement statistics

	*Pf*PYK-OX/ATP
PDB ID	6KSH
Data collection	
Space group	P 6_1 2 2
Cell dimensions	
a, b, c (Å)	139.41, 139.41, 453.16
α, β, γ (°)	90.00,90.00,120.00
Solvent content (%)	57
Resolution (Å)	60.37-2.60
No. of measured reflections[a]	1695738 (251897)
No. of unique reflections	81169 (11640)
Wilson B-factor (Å^2)	58.4
R_{merge} (%)	19.0 (131.9)
I/σI	15.4 (3.1)
CC (1/2)	0.998 (0.803)
Completeness (%)	100.0 (100.0)
Multiplicity	20.9 (21.6)
Refinement	
Monomers in a.u.	4
No. reflections	81001
R_{work} / R_{free}	0.2072/0.1529
No. of non-H atoms	
Protein	14985
Water	950
Ligands	160
Average B-factor (Å^2)	
Protein	55.2
Water	54.1
Ligands	50.9
RMS deviations	
Bond lengths (Å)	0.010
Bond angles (°)	1.25
Ramachandran plots	
Favoured (%)	97.5
Allowed (%)	99.5

[a]The numbers in parentheses refer to the last (highest) resolution shell.

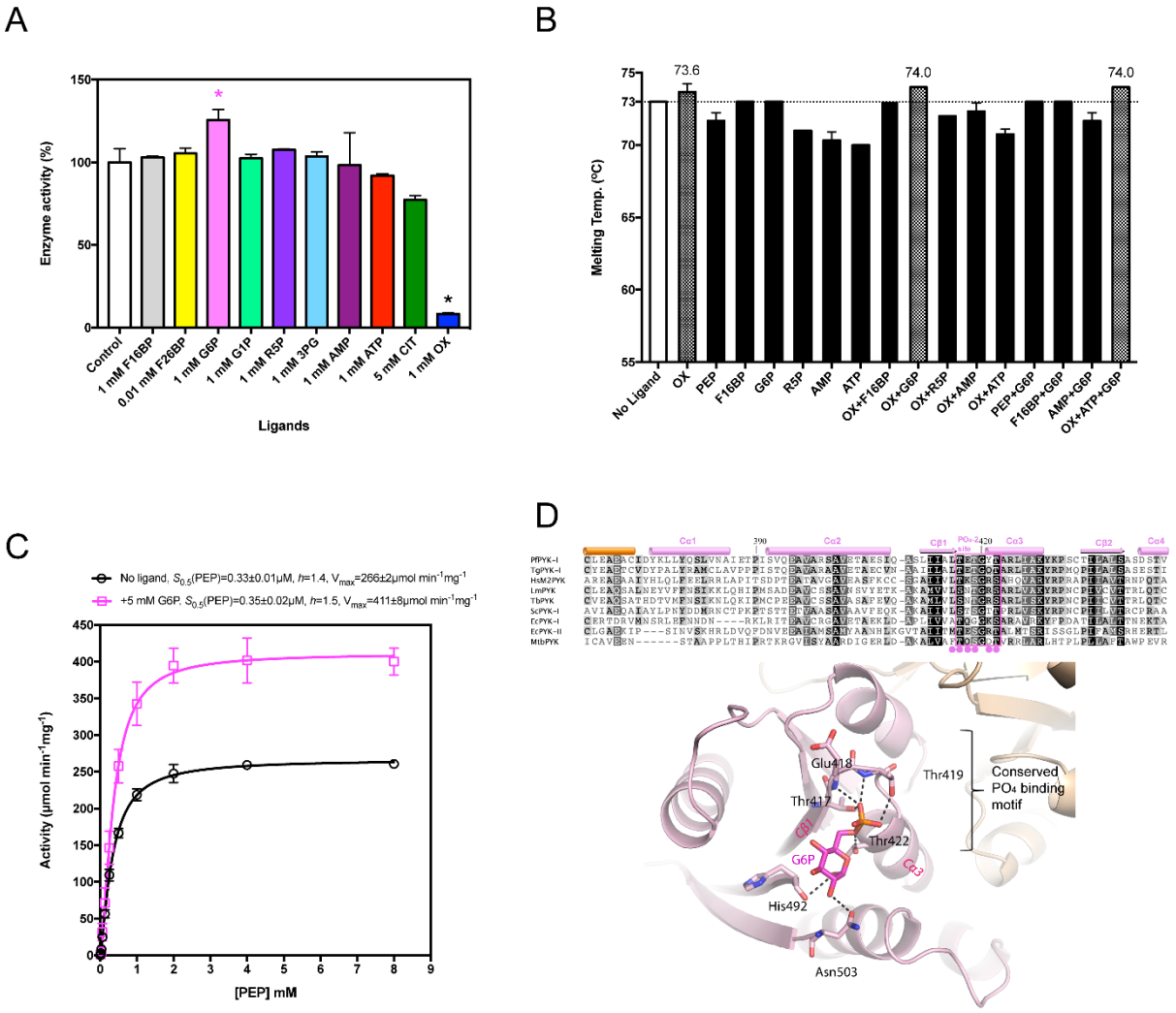

Fig. 1. Modulation of *Pf*PYK activity. (**A**) Regulation of *Pf*PYK activity by small molecules. The magenta and black asterisks indicate ligands having the significant impact on enzyme activation or inhibition, respectively. Data represent mean ± SD for N=3 experiments. (**B**) Stabilisation of *Pf*PYK by small molecules binding. The T_m values above 73 °C (no ligand) are highlighted. Data represent deviation about the mean for N=2. (**C**) Concentration-response curves observed for titration of PEP against *Pf*PYK activity in the absence or presence of G6P. Data represent mean ± SD for N=4. (**D**) The proposed binding mode of G6P at the effector site derived from docking with "AutoDock". Partial amino-acid sequence alignment of the effector site among PYKs is shown above the structure model. The amino acids involved in the effector binding (magenta circles) are indicated below the aligned sequences.

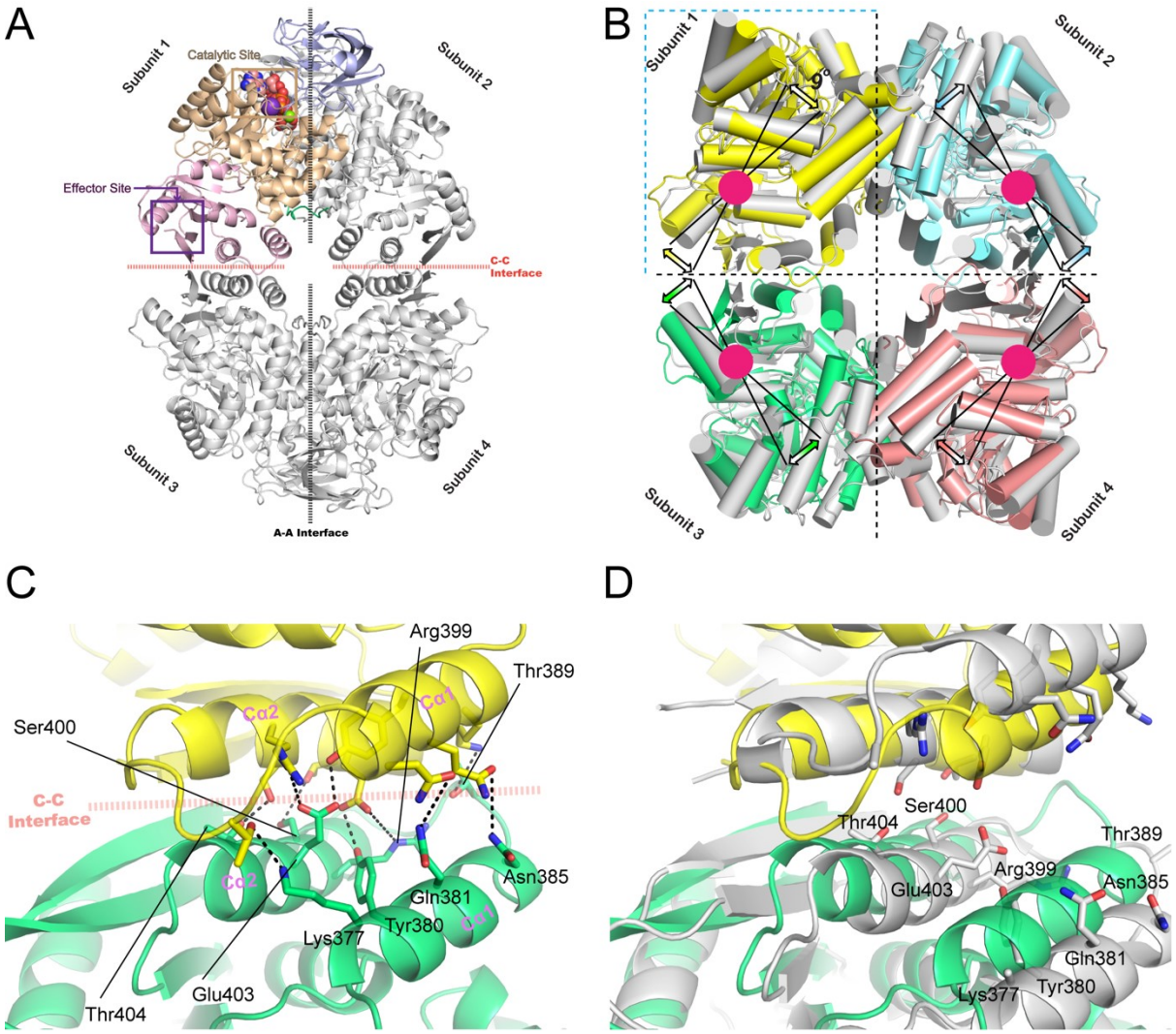

Fig. 2. Structure of *Pf*PYK and overview of allosteric conformational changes. (**A**) Overall view of the *Pf*PYK tetramer from the crystal structure. Each monomer comprises four domains shown in different colours: N-terminus in green (residues 1-28), A-domain in brown (residues 29-105, 204-375), B-domain in blue (residues 106-203), C-domain in pink (residues 376-511). The polypeptide chains are shown as ribbons while ligands and metals are shown as spheres. (**B**) Rigid-body rotation occurring during the transition between the T- (PDB ID: 3KHD) and R- (PDB ID: 6KSH) state of *Pf*PYK. The transition between the T- (grey) and R-state is accompanied by a 9° rigid-body (AC core) rotation around the central pivot. (**C**) Interactions at the C-C interface between subunit 1 and subunit 3 in the R-

state of *Pf*PYK. Residues from subunit 3 involved in interface interactions are highlighted. (**D**) Comparison of the C-C interface between the T- and R-state of *Pf*PYK.

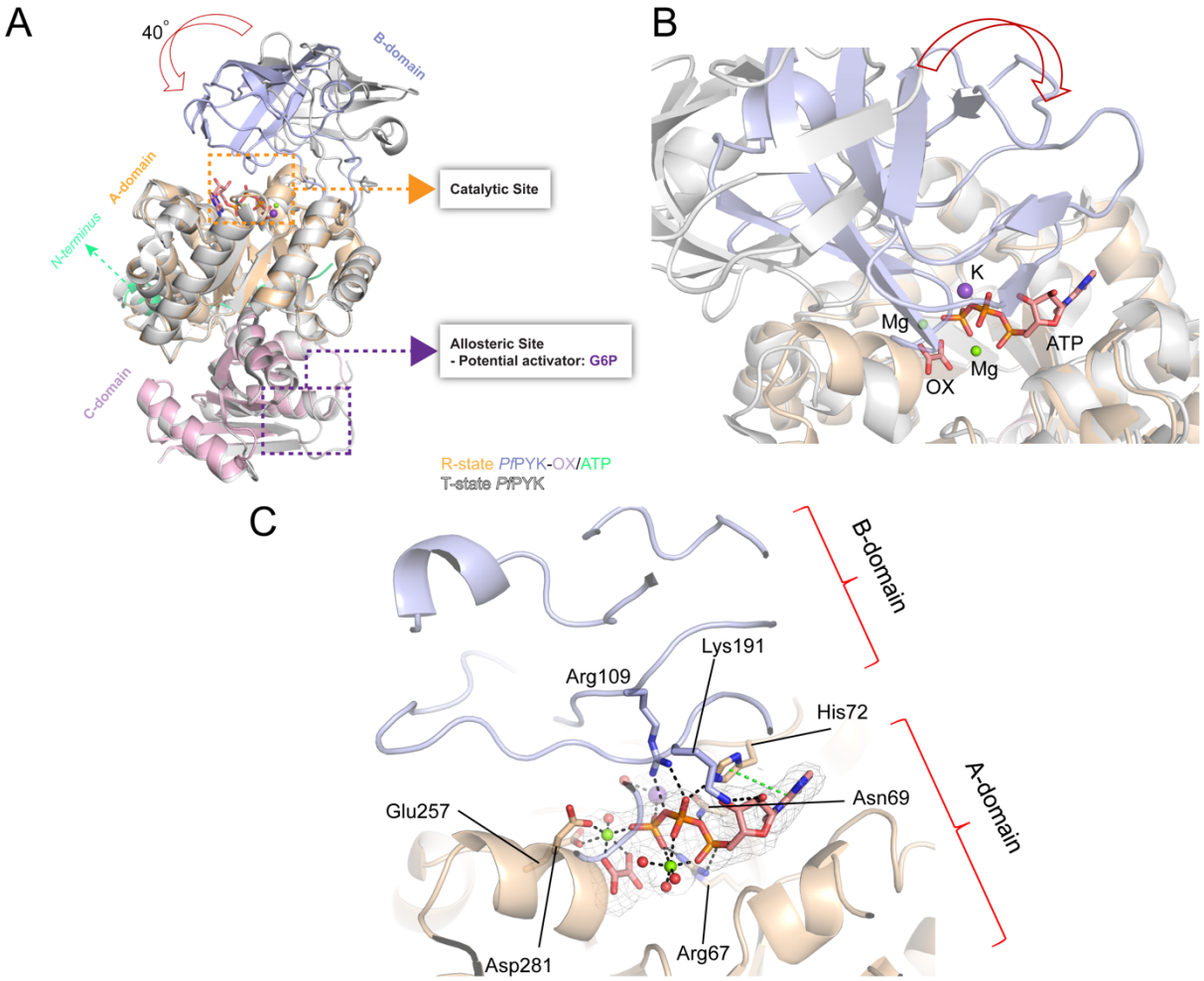

Fig. 3. B-domain of *Pf*PYK adopts a closed conformation to accommodate active-site ligands. (**A**) Subunits from two *Pf*PYK structures (chain D in each structure) are superposed based on the AC-core, to show the relative movements of the B-domains: R-state *Pf*PYK-OX/ATP (PDB ID: 6KSH) and T-state *Pf*PYK (PDB ID: 3KHD). (**B**) Enlargement of the catalytic site showing that the B-domain is in a closed conformation, when active-site ligands are bound. (**C**) Active-site interactions in the *Pf*PYK-OX/ATP structure. The presence of ATP, oxalate and metal ions is documented by an unbiased *Fo-Fc* electron density map (grey) contoured at 3σ.

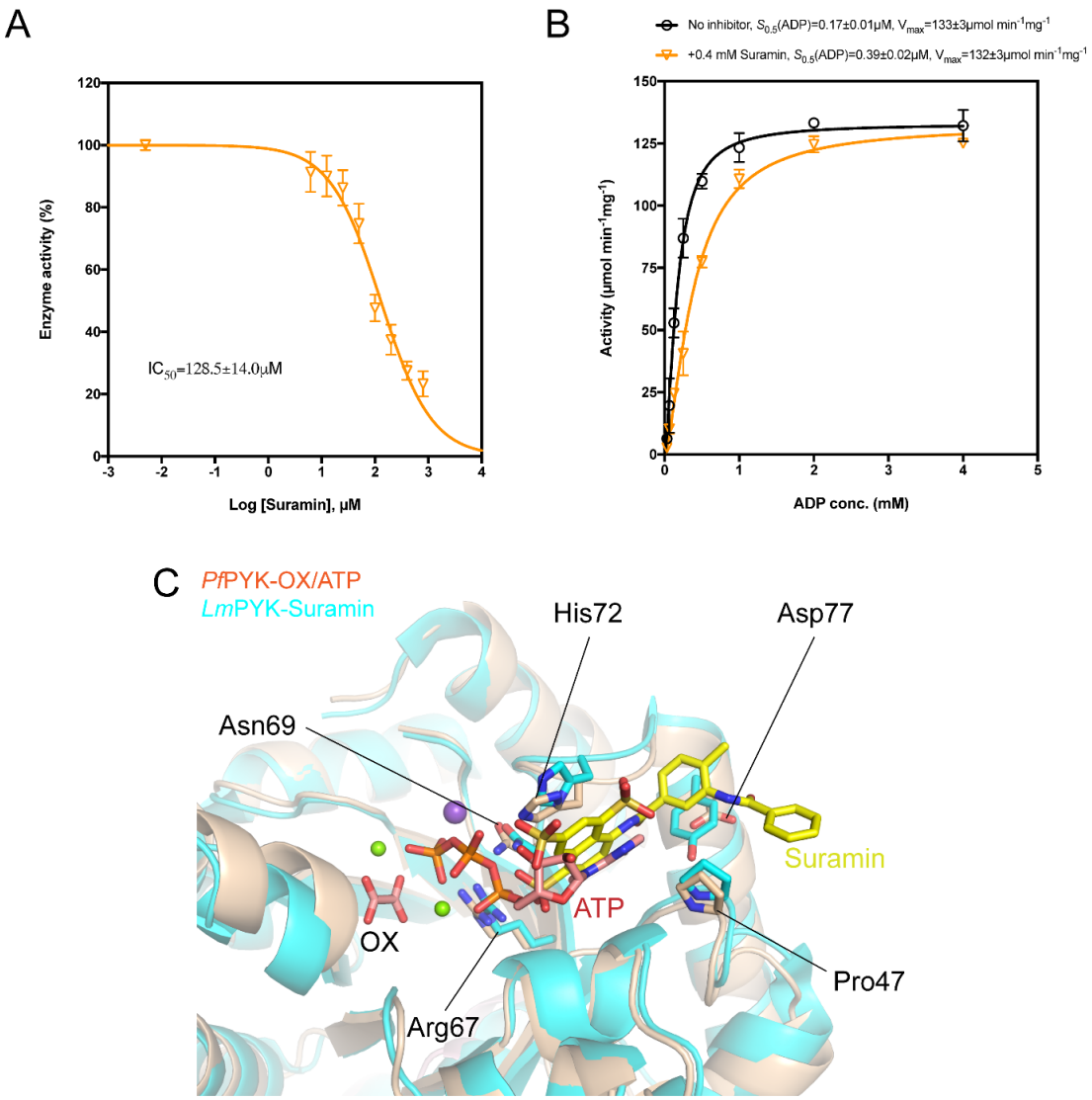

Fig. 4. The drug suramin inhibits *Pf*PYK by competing with substrate ADP. (**A**) Dose-dependent inhibition of *Pf*PYK by suramin. Data represent mean ± SD for N=4. (**B**) Concentration–response curves observed for titration of ADP against *Pf*PYK activity in the absence and presence of suramin. Data represent deviation about the mean for N=2. (**C**) Suramin and ATP are proposed to share an overlapping binding site. OX/ATP-bond *Pf*PYK (PDB ID: 6KSH) was superimposed onto the suramin-bound *Leishmania mexicana* PYK (*Lm*PYK; PDB ID: 3PP7) structure, based on superposition of their Cα atoms.